27th ABCM International Congress of Mechanical Engineering
December 04-08, 2023, Florianópolis-SC, Brazil

COB-2023-1652
Notched Strength of Woven Reinforcement Composites Under Mixed-Mode In-Plane Loading

Felipe Ruivo Fuga
Maurício Vicente Donadon
Instituto Tecnológico de Aeronáutica - ITA, São José Dos Campos/SP - Brazil
fuga@ita.br / donadon@ita.br

Abstract. *The ever-growing use of fibre reinforced composites as primary structural components within the aerospace industry has required more accurate models for predicting failure. While on the one hand experimental validation is still necessary, specially for composite manufactured parts, on the other, time and budget consuming test campaigns are employed. Therefore, research has played an important role in the development of efficient yet safe structures. For the maximum load bearing capacity of a structural member, different approaches can be employed. Most commonly, stress analyses are employed to determine critical values and regions. While this approach can be sufficient for regions with small stress gradients, it might not be enough for notched members, for example. In such cases, crack stability analysis is usually carried out, from which the maximum load capacity can be determined. There is however a lack of data and analysis on the fracture behavior under mixed-mode in-plane loading, for fibre reinforced composites. Therefore, this paper provides experimental data on the mixed-mode behaviour of woven fabric reinforced thermoset composite specimens, using a Modified Arcan Fixture for mixed-mode testing. Specimens were manufactured by the Resin Transfer Moulding process and machined. Digital Image Correlation technique was used to measure the normal and shear strain fields along the notched length, allowing for a stress intensity factor to be determined. Maximum load as a function of loading angles presented a correlation with predictions for fracture dominated behaviour for opening modes only and stress failure criteria for sliding modes. Proposed criterion requires as input parameters, critical stress intensity factors and strength values, only. These results justify the development of such criterion to be implemented on user material models for finite element analysis, and high-fidelity virtual testing campaigns.*

Keywords:*Fracture Mechanics, Mixed-mode Fracture, Composite Structures.*

1. INTRODUCTION

Structural engineers seeking efficient design solutions are constantly searching for a balance between allowable stresses, to prevent any relevant failure behaviour, and the overall structural weight. Aerospace industry, for example, requires efficient structural designs as the payload cost per kilogram is much higher than other transport industries, such as automotive and naval. For this task, specifically, composite materials bring the potential of optimization due to their weight-specific material properties. However, optimum design parameters are difficult to be achieved as a deep understanding on the failure analysis of structures and high confidence on material properties are required.

Failure in continuous fibre-reinforced composites are usually described in terms of interlaminar failure, associated with delamination, and intralaminar failure regarding matrix cracking and fibre breakage. For many in-plane loading applications, the maximum load bearing capacity of a composite structure is directly associated with intralaminar modes, as the fibres are subjected to most of the external loads. While many stress based failure criteria were developed to predict failure under bi-axial and even tri-axial stress states, they prove to be inaccurate in the presence of stress raisers, such as notches or sudden geometry variations. Moreover, the application of stress concentration factors, in an attempt to predict maximum stresses on a notched structure may lead to infinite stresses at the notch/crack tip. Therefore, some concepts of Fracture Mechanics, such as the Stress Intensity Factor (SIF) and Strain Energy Release Rate (SERR) allowed for designers to predict not only maximum load bearing capacity, but also the crack evolution. Experimental evidence of the existence of an energy driven Fracture Criterion has been provided by Laffan *et al.* (2012, 2013); Blanco *et al.* (2014); Souza *et al.* (2019); Xu *et al.* (2021) with tests performed on Compact Tension specimens under Mode I. Buczek and Herakovich (1985) showed that for off-axis notched specimens under tension, maximum tangential stress criterion would accurately predict crack direction, and cracks propagated parallel to the fibre direction, as the ratio between stresses in the matrix direction and respective strength is close to unity. These results were once again evaluated by Cahill *et al.* (2014) where an experimental campaign on notched specimens and numerical models using the extended finite element method showed similar results. However, woven fabric composites, fracture behaviour is not as simple, as an interaction between warp and weft exists. For the interaction between opening and in-plane sliding modes, I and II respectively, far less experimental data is available in the scientific literature and the overall interaction behaviour is still a subject of research. An overview on experimental methods and results is presented as a systematic review by Monticeli *et al.* (2023).

Currently, on of the most popular testing set-up is derived from a test method proposed by (Arcan *et al.*, 1978) in the late 70s. The author proposed a test configuration to produce uniform plane stress at a significant specimen section, by the application of a single tensile load applied off-axis relative to fibre directions. Compared to the alternative, rail shear configuration from ASTM D7078, where the specimen is assembled between parallel fixtures, the proposed new method displays the advantage of producing pure shear loads. Picture-frame fixtures are also discussed by the author, where the main disadvantage is related to the statically indeterminate normal stresses developed under shear configurations. For the aforementioned reasons, the proposed testing set-up became popular and has been addressed as Arcan fixture, in the scientific literature. Further development lead to the optimization of the Arcan fixture, where similar specimens are assembled in off-axis orientation to the applied load, and are called Modified Arcan Fixtures (MAFs). In this application, the manufacturing process of specimens is drastically simplified, and specimen geometry can be chosen as required. Some relevant configurations to mixed-mode fracture testing are the Compact Tension Shear (CTS) and V-notch geometries, derived from ASTM Standards for Mode I fracture and shear characterization, ASTM E399 and ASTM D5379, respectively. Rikards *et al.* (1998); Nikbakht and Choupani (2008); Cognard *et al.* (2011); Boyina *et al.* (2014); Malyszko and Rutkiewicz (2017); Gan *et al.* (2018); Din *et al.* (2020); Ud Din *et al.* (2020) showcase MAF applications to composite Mixed-Mode fracture testing.

Within this context, this study aims to provide experimental data on the interaction between normal and tangential stresses for woven fabric composite specimens under static mixed-mode loading in the presence of a stress raiser and describe the failure mechanisms associated.

2. MATERIALS AND METHODS

2.1 Specimen design

As the presence of stress raisers lead to singularities in the stress field, a notched specimen is desired, to evaluate the maximum load bearing capacity of the structure. Therefore a V-notched specimen with an additional longitudinal notch was manufactured as displayed in Fig. 1a. The additional notch was introduced to increase the stress concentration at the crack tip, as the V-notch geometry provides a continuous cross-sectional transition, rather than discrete. Moreover, this notch was manually created with a saw of approximately 1 mm width and a total length of approximately 3mm on each side. Fig. 1a also displays dimensions w' and w with average values of $20mm$ and $26mm$, respectively. For all following calculations, width and notch length values for each specimen were used, rather than the average. Specimens were manufactured by the Resin Transfer Moulding (RTM) process, with woven carbon fabric reinforcement Hexcel AGP-193 and thermoset Epoxy matrix Araldite LY5052 and a $[0]_8$ layup, and average ply thickness of $0.25mm$. This particular layup was chosen, to ensure the decomposition of normal stresses along and parallel the fibre directions. All specimens followed a post-cure cycle with 24 hours at $100°C$ and were obtained from the same manufacturing batch. Fig. 1a also displays Aluminium reinforcement tabs that were adhered to the specimen surface, to contain the influence of shear deformation around the bolted fixtures.

2.2 Mixed-Mode testing

A Modified Arcan Fixture was designed for the application of both normal and tangential stresses on notched specimens, as displayed in Fig. 1b, where the external prescribed load is represented by F and is applied at an off-axis angle θ with respect to the specimens critical ligament width w. Internal normal and tangential forces, F_n and F_t, respectively, develop along the specimens cross section, with a compound magnitude equal and opposite to F. Eqs. 1 and 2 represent the average stresses σ and τ on the cross section, with an overall thickness of t and ligament width of w, as a function of loading angle θ. Moreover, the average normal and tangential strengths can be determined by Eqs. 3 and 4, as long as the loading angle θ and maximum load at that angle F^{max} are known values.

$$\sigma(\theta) = \frac{F cos\theta}{wt} \quad (1)$$

$$\tau(\theta) = \frac{F sin\theta}{wt} \quad (2)$$

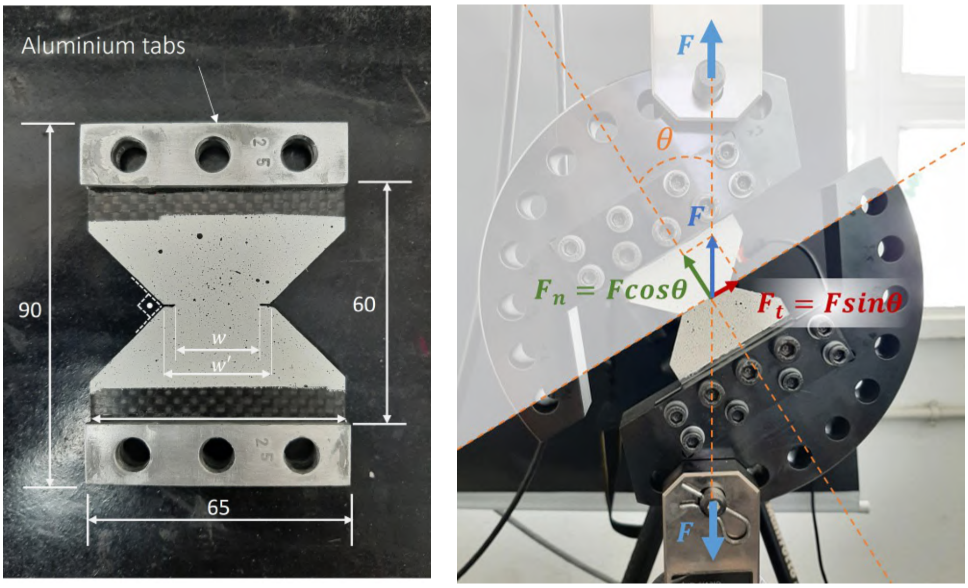

(a) Specimen geometry (b) Internal load decomposition

$$S_0^\theta = \frac{F^{max} cos\theta}{wt} \tag{3}$$

$$S_{\frac{\pi}{2}}^\theta = \frac{F^{max} sin\theta}{wt} \tag{4}$$

Therefore, specimen strength, representing the maximum load bearing capacity, is represented by a normal component (S_0) and a tangential ($S_{\frac{\pi}{2}}$), which may be a function of the stress ratio σ/τ, dependent on loading angle θ. To evaluate the change in average strength as a function of stress ratio, specimens were positioned at four different loading angle configurations, as displayed in Fig. 1, for angles varying from 0° to 90° with 30° increments. The MAF loading device was assembled into an MTS hydraulic testing machine on standard

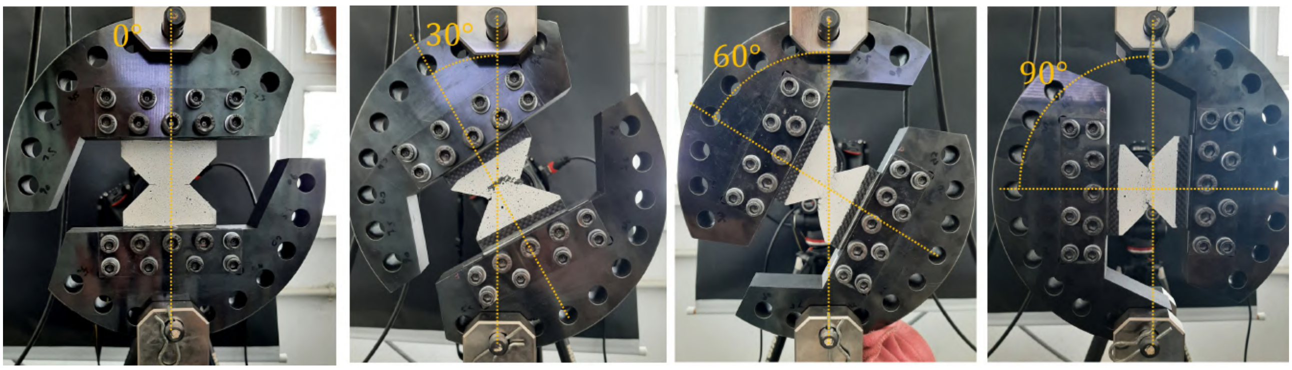

Figure 1: Loading angle configurations [0/30/60/90]

MTS 640 Fracture Mechanics Clevis Grips. In an attempt to record stable crack propagation, a displacement controlled test was carried out rather then load controlled. A 100kN load cell provided the load history.

2.3 Strain Field and Stress Intensity Factors

Additionally to the global variables of load and displacement, strain-field throughout the domain was measured using the Digital Image Correlation Technique (DIC). For the DIC analysis, a speckle patter was beforehand painted on specimen surfaces so that representative facet cells could be defined and displacement could be tracked at any instant. For this test campaign GOM Correlate DIC software was used for the correlation algorithm. A camera was positioned perpendicular to the specimens frontal plane and a video-file recorded the test. An algorithm was implemented in Python to extract the images at the any given test instant and compared to the corresponding load and displacement values. Facet size and overall mesh can be seen in Fig. 2, for one specimen. The image also displays the vertical strain-field $\epsilon_{yy}(x, y)$ for a test with $\theta = 0°$, which corresponds to the material direction 1 (ϵ_{11}).

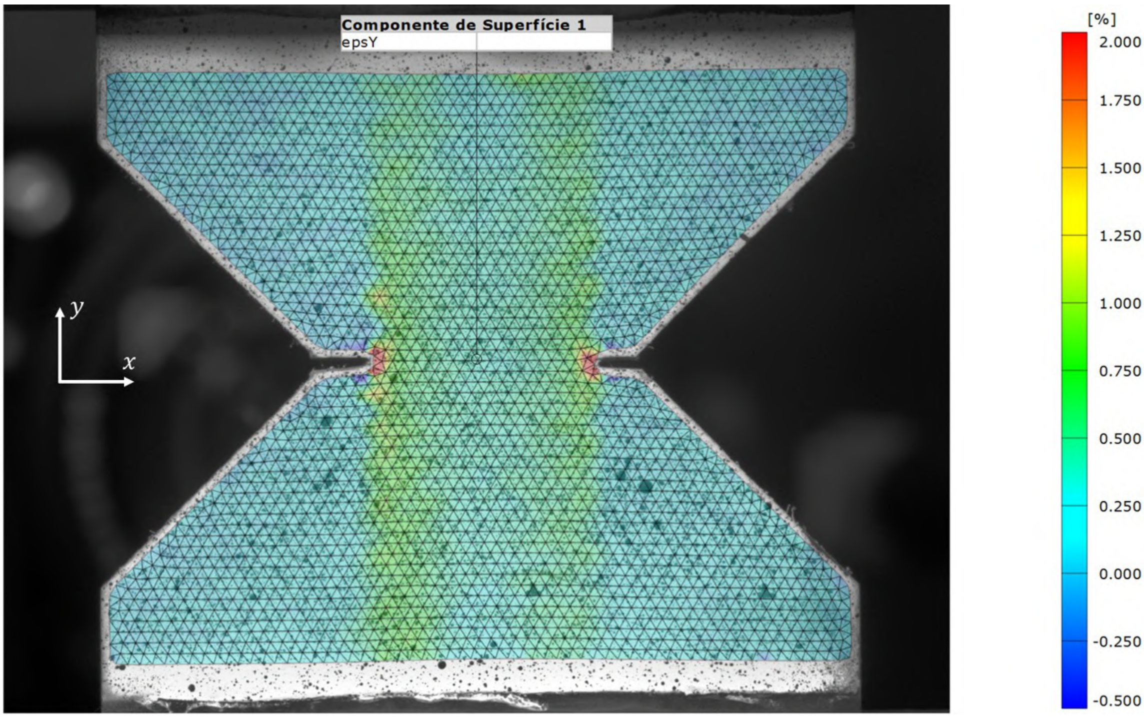

Figure 2: DIC mesh - Vertical strain component

Monitoring of strain-field during along the test allows for stress intensity factors to be determined ahead of the notch. SIF are commonly reported as a function of far-field stresses σ and τ and a finite body interaction term β, which for composite materials is a function of both geometry and material properties, resulting in Eqs. 5 and 6. With known far-field stresses ans SIF, β can be calculated.

$$K_I = \sigma\sqrt{\pi a}\beta_I \tag{5}$$

$$K_{II} = \tau\sqrt{\pi a}\beta_{II} \tag{6}$$

DIC allows for strain-field distribution to be evaluated throughout the specimen domain. Assuming Williams (Williams, 1961), first term expansion for the normal stress distribution ahead of a crack tip, along a longitudinal distance x, the local stress field becomes

$$\sigma(x) = \frac{K_I}{\sqrt{2\pi x}}. \tag{7}$$

This expression is valid as long as the material is orthotropic, with orthotropy and notch directions aligned, and stress-field is evaluated along a a horizontal line representing the distance from notch-tip. This condition is attended for a $[0]_8$ laminate of plain weave reinforcement. Introducing the constitutive relation for the material, the strain-field can be described in terms of the singular term (SIF), at any given load.

$$\epsilon(x) = \frac{K_I(1 - \nu_{12}\nu_{21})}{E_1\sqrt{2\pi x}} \tag{8}$$

Therefore, stress intensity factors at any given load are obtained directly from a best-fit for the strain-field resulting from the DIC analysis. Calculated SIF's can be substituted back into Eqs. 5 and 6, allowing for β factors to be determined.

3. RESULTS

Fig. 3 displays load versus displacement plots, showcasing the relationship between loading angle and non-linearity as well as the maximum load. It is evident that an increase in loading angle leads to a simultaneous increase in non-linearity and a decrease in the maximum load. This increase in non-linearity can be attributed to the specimens being subjected to higher tangential (shear) stresses compared to normal stresses. The same effect is observed for $\theta = 0°$ as the load approaches 12kN. Load increments are not linearly related to displacement increments any more, until the maximum load is achieved. This behaviour is attributed to the slight specimen eccentricity, as two notches were introduced. At high enough load values, one specimen side displays an opening greater than the other, shifting the actual center of the width w. Specimens tested at 60° and 90° displayed a considerable degree of distortion, related to shear strains, without reaching a load at which complete fracture happens. Many small cracks developed under shear dominated modes, but the overall behaviour indicates that the complete section failed due to excessive straining. Conversely, specimens tested at 0° and 30° exhibited unstable fracture, resulting from a sudden increase in crack length leading to separation.

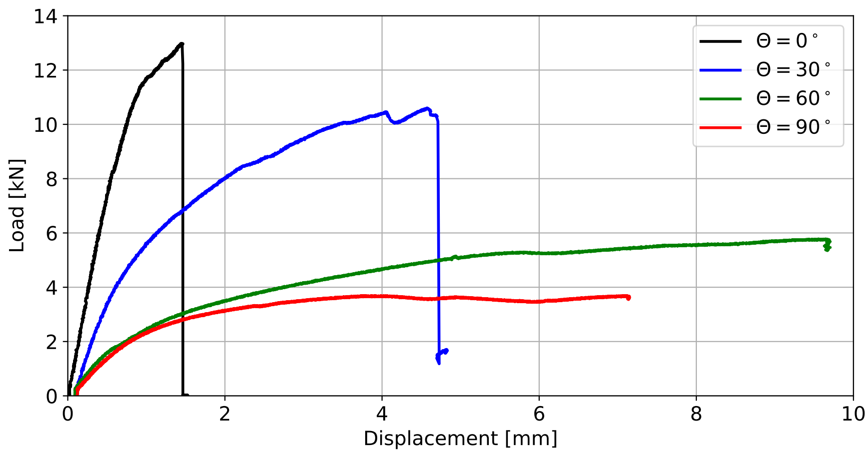

Figure 3: Load versus displacement for different loading angles θ

At $\theta = 0°$, Mode I loading, the specimen fractured along a straight line across the ligament width w, as showed in Fig. 4. Despite the displacement controlled testing strategy, crack propagated suddenly resulting in the complete specimen separation. Similarly crack propagation was unstable for the specimen at $\theta = 30°$ and resulted in a curved path of surface separation. In this particular loading configuration, there were only few fibres that remained connected between the upper and lower portions of the specimen, thereby preventing complete separation during the test. Nevertheless, this effect can be considered insignificant since the majority of the surface area exhibited separation.

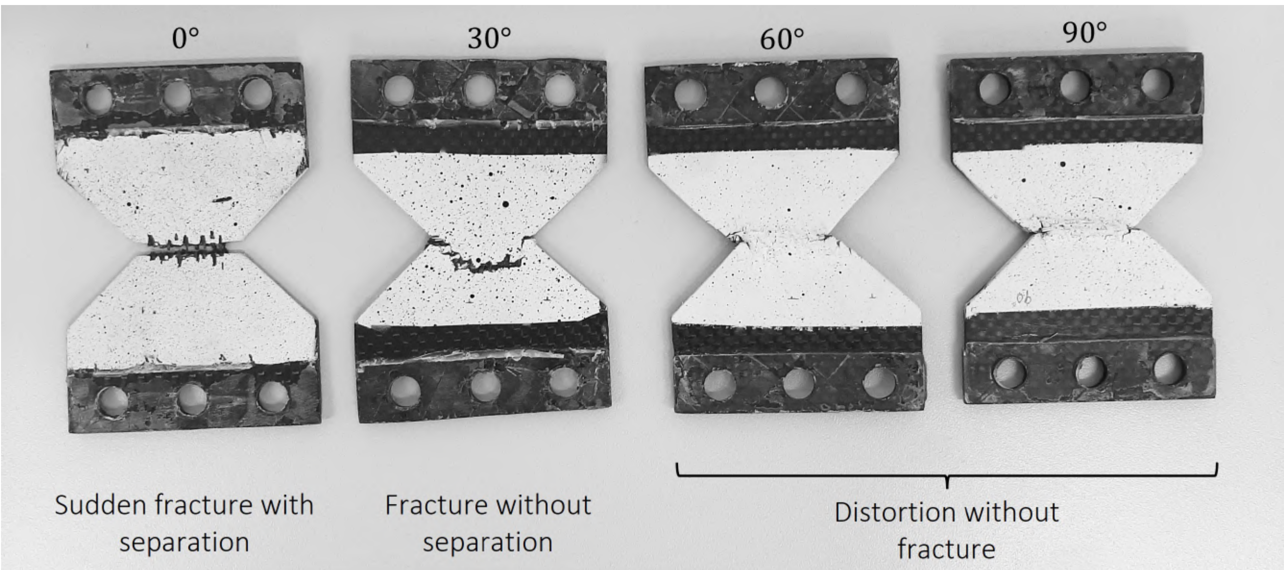

Figure 4: Failure characteristics for different angles

Maximum in-plane principal strain fields are shown in Figures 5a to 5d, for each loading configuration.

Principal strain component is displayed as all in-plane components are taken into account. For Figure 5a, the strain-field displays a region of expressive strain concentration at the notch tip. However, shear deformation bands above and below the notch are also visible. For all other off-axis loading configurations a shear band, defined as a region subjected mostly to shear strains, is formed along the specimen width. DIC analysis indicates that shear strain magnitude increases rapidly as the off-axis angle increases. In the images, maximum in-plane principal strain directions are represented by the arrows, over the mesh grid. As the loading angle increases, the directions change from approximately vertical, to a 45° degree direction, indicating that shear strains are in fact much grater than the other components.

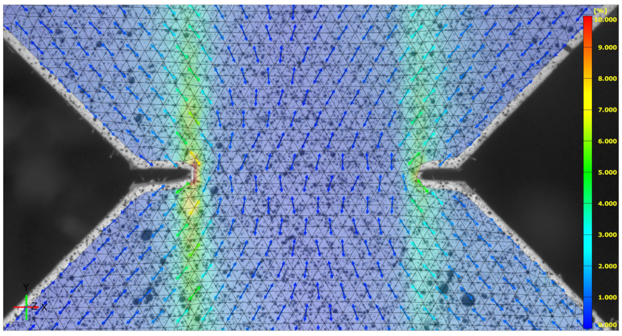

(a) Maximum in-plane principal strain-field - 0°

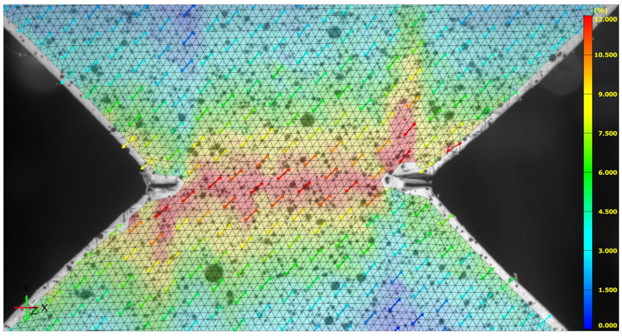

(b) Maximum in-plane principal strain-field - 30°

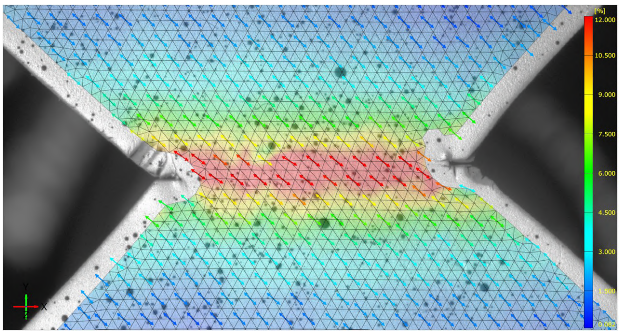

(c) Maximum in-plane principal strain-field - 60°

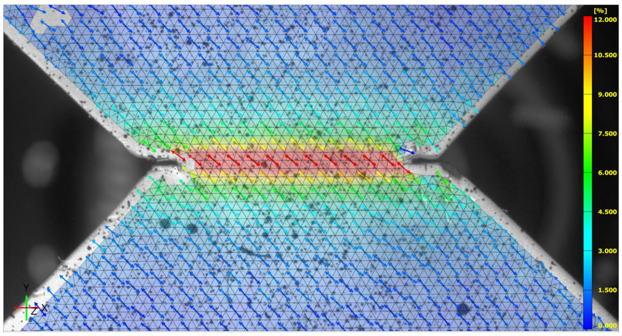

(d) Maximum in-plane principal strain-field - 90°

Figure 5: Maximum principal strain values and directions

3.1 Mode I failure

Apparent strength for Mode I test is computed from Eq. 3, resulting in $S_0 = 326.6MPa$, which is approximately half of the material strength obtained from a tensile test, $X = 730MPa$. Therefore, the limiting factor for the load bearing capacity is related to the propagation of the crack. Aiming to characterize the fracture toughness, SIFs were obtained from the DIC normal strain-field, represented by the points in Figure 6a. This plot showcases that an approximately constant strain value is obtained at a distance from the each notch tip, and a singular field describes the near crack-tip stain-field. Therefore, in a region between 0 and 2 mm ahead of the crack tip, the parameter K_I for any given load was calculated, for a best-fit under a single parameter over Equation 8. Figure 6b shows the fitted curves with a $1/\sqrt{r}$ singularity, which correlate well with experimental points in the limit where $r \to 0$.

The analysis resulted in a linear relation between SIF and applied load F, where $K_I \approx 0.12F_{kN}$, and a critical SIF value of $K_{I_c} = 1560MPa\sqrt{mm}$. Substituting the ratio between SIF and load in Eq. 5, $\beta_I = 1.23$ for the configuration under mode I loading. These values are necessary to predict the allowable normal far-field stress σ at the maximum load under mode I, which is the apparent strength S_0. In conclusion, Mode I strength can be well estimated using Eq 5 and the aforementioned parameters, resulting in a predicted strength of 332.6 MPa, which is within 2% of the experimental value.

3.2 Mode II

Mode II loading, $\theta = 90°$, resulted in a non-linear relation between load and displacement. This behaviour is expected as the in-plane constitutive shear response exhibits an elastoplastic behaviour. Figure 7 shows the evolution o in-plane shear strain ϵ_{xy}, that for this layup coincides with local directions ϵ_{12}. From the plots it is clear that due to the reduced constitutive stiffness under shear, the material is not sensitive to notches. This

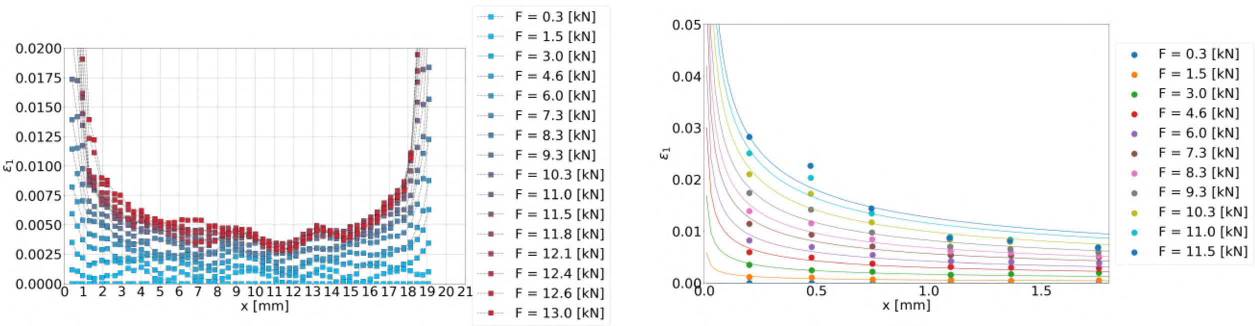

(a) Vertical strain component along crack line (b) $1/\sqrt{r}$ adjusted curves for experimental data

Figure 6: ϵ_{11} as a function of distance x

characteristic can also be assessed from the strain-field profile in Fig. 5d. The specimen strength calculated from Eq. 4 results in $S_{\frac{\pi}{2}} = 88MPa$, while the maximum shear stress obtained from a shear characterization material test provides an in-plane strength of $S_{12} \approx 100MPa$. Therefore, experimental data suggest that the introduction of notches play small roles in this specimen configuration, and strength can be estimated by a stress limit approach rather than Eq 6.

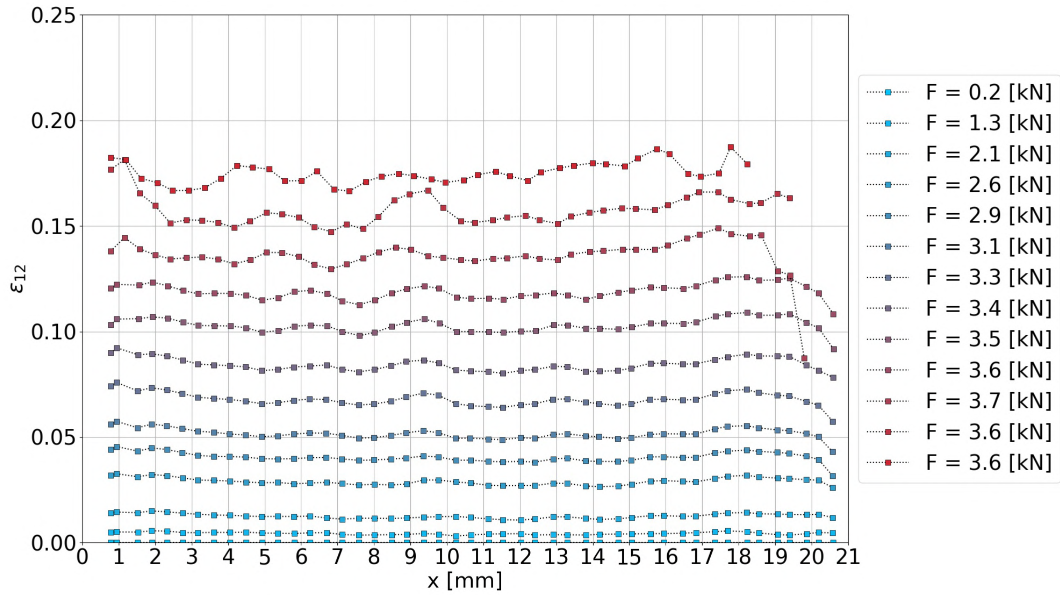

Figure 7: In-plane shear strain evolution

3.3 Mixed-Mode

Under mixed-mode loading, a simple failure condition could be evaluated, where the ratio between the acting stress components and the maximum allowable normal and tangential stresses (strengths) define the maximum load bearing capacity. Fig. 8a shows the correlation between the maximum allowable normal and tangential section forces and experimental points, as a function of the loading angle θ. As the angle increases, actuating normal forces are decreased in proportion to $1/cos\theta$, while tangential ones increase by $1/sin\theta$. Therefore, the maximum allowable load, represented by the blue dashed line increases while the other component, represented by the green dashed line, decreases. Both lines are obtained from Eqs. 9 and 10. Experimental data appears to be contained in a region defined by the minimum strength between the two lines, described by Eq. 11. To represent in terms of applied load, the strength is multiplied by the cross sectional area wt.

$$\overline{S_0} = \frac{K_{I_c} wt}{cos\theta\sqrt{\pi a}} \tag{9}$$

$$\overline{S_{\frac{\pi}{2}}} = \frac{\tau_{12} wt}{sin\theta} \tag{10}$$

$$\overline{S} = min\left(\frac{K_{I_c} wt}{cos\theta\sqrt{\pi a}}, \frac{\tau_{12} wt}{sin\theta}\right) \tag{11}$$

Parameter θ on the denominator, in Eqs. 9 and 10, provides an increase in the apparent strength, for the MAF loading device. However, the physical meaning of the proposed method consists of a constant fracture toughness value K_{I_c} and a constant in-plane shear stress value τ_{12}. The apparent strength increase is dependent on the loading angle configuration, while the material strengths are not. When plotting the corresponding normal and tangential stresses on a τ x σ plot, the allowable design space becomes a rectangular portion, as in Fig. 8b, representing a non-interactive criterion.

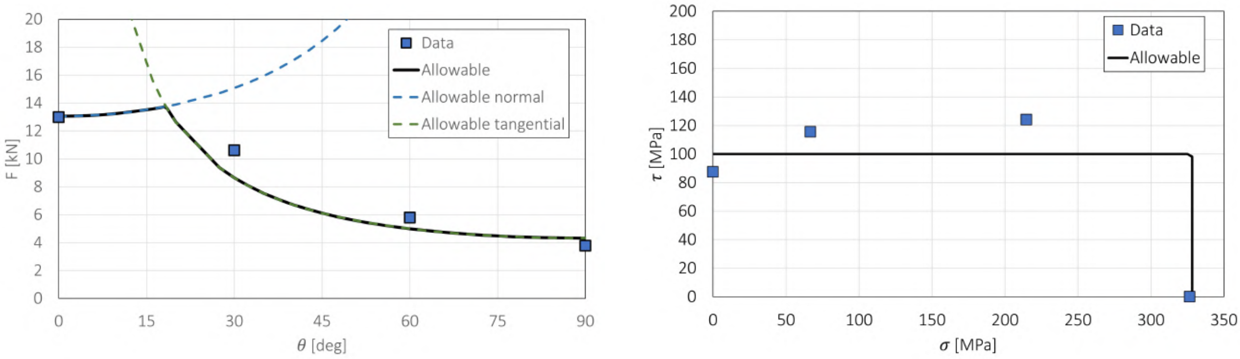

(a) Maximum load relation to angle θ

(b) Maximum stress components envelope

Figure 8: Strength values for experimental data and criterion

4. CONCLUSIONS

This paper presented the application of a MAF fixture to assess the maximum load capacity of notched woven composite specimens. The loading device served as a reliable testbed for evaluating failure criteria when subjected to combined tensile and shear load conditions. Additionally, the testing procedure enabled the monitoring of strain fields through point tracking and image digital correlation algorithms. The experimental data exhibited variations in the maximum load-bearing capacity, with a decreasing trend observed as the off-axis angle increased. Analysis of the failure modes indicated that failure under normal stresses led to an increase in crack length, while failure under tangential stresses resulted in angular distortion until secondary cracks formed. Consequently, a criterion was proposed for predicting strength, involving the evaluation of minimum strengths along each direction based on fracture mechanics criterion for opening mode and stress criterion for sliding. The proposed method, though simple, showed a reasonable correlation with the experimental data. To further enhance this work, it is suggested to introduce testing configurations at different angles, such as 15 degrees, which could either validate or expose the limitations of the proposed methodology. This test campaign is part of a broader ongoing experimental study encompassing different specimen configurations.

5. ACKNOWLEDGEMENTS

This study was financed in part by the Coordenação de Aperfeiçoamento de Pessoal de Nível Superior - Brasil (CAPES) - Finance Code 001 and CNPq Grant (No. 301069/2019-0).

6. REFERENCES

Arcan, M., Hashin, Z. and Voloshin, A., 1978. “A method to produce uniform plane-stress states with applications to fiber-reinforced materials - A specially designed specimen yields material properties under pure shear or uniform plane-stress conditions”. *Experimental Mechanics*, Vol. 18, No. 4, pp. 141–146. ISSN 00144851.

ASTM D5379, 2021. “Standard Test Method for Shear Properties of Composite Materials by the V-Notched Beam Method”. Standard, American Society for Testing Materials International, West Conshohocken, PA.

ASTM D7078, 2012. “StandardTest Method for Shear Properties of Composite Materials by V-Notched Rail”. Standard, American Society for Testing Materials International, West Conshohocken, PA.

ASTM E399, 2022. “Standard Test Method for Linear-Elastic Plane-Strain Fracture Toughness of Metallic Materials”. Standard, American Society for Testing Materials International, West Conshohocken, PA.

Blanco, N., Trias, D., Pinho, S.T. and Robinson, P., 2014. “Intralaminar fracture toughness characterisation of woven composite laminates. Part I: Design and analysis of a compact tension (CT) specimen”. *Engineering Fracture Mechanics*, Vol. 131, pp. 349–360. ISSN 00137944.

Boyina, D., Banerjee, A. and Velmurugan, R., 2014. "Mixed-mode translaminar fracture of plain-weave composites". *Composites Part B: Engineering*, pp. 21–28. ISSN 13598368.

Buczek, M. and Herakovich, C., 1985. "A Normal Stress Criterion for Crack Extension Direction in Orthotropic Composite Materials". *Journal of Composite Materials*, Vol. 19, No. 6, pp. 544–553. ISSN 0021-9983.

Cahill, L.M., Natarajan, S., Bordas, S.P., O'Higgins, R.M. and McCarthy, C.T., 2014. "An experimental/numerical investigation into the main driving force for crack propagation in uni-directional fibre-reinforced composite laminae". *Composite Structures*, Vol. 107, No. 1, pp. 119–130. ISSN 02638223.

Cognard, J.Y., Sohier, L. and Davies, P., 2011. "A modified Arcan test to analyze the behavior of composites and their assemblies under out-of-plane loadings". *Composites Part A: Applied Science and Manufacturing*, Vol. 42, No. 1, pp. 111–121. ISSN 1359835X.

Din, I.U., Tu, S., Hao, P., Panier, S., Khan, K.A., Umer, R., Shah, S.Z., Franz, G. and Aamir, M., 2020. "Sequential damage study induced in fiber reinforced composites by shear and tensile stress using a newly developed Arcan fixture". *Journal of Materials Research and Technology*, Vol. 9, No. 6, pp. 13352–13364. ISSN 22387854.

Gan, K.W., Laux, T., Taher, S.T., Dulieu-Barton, J.M. and Thomsen, O.T., 2018. "A novel fixture for determining the tension/compression-shear failure envelope of multidirectional composite laminates". *Composite Structures*, Vol. 184, No. October 2017, pp. 662–673. ISSN 02638223. doi:10.1016/j.compstruct.2017.10.030.

Laffan, M., Pinho, S. and Robinson, P., 2013. "Mixed-mode translaminar fracture of CFRP: Failure analysis and fractography". *Composite Structures*, Vol. 95, pp. 135–141. ISSN 02638223.

Laffan, M., Pinho, S., Robinson, P. and McMillan, A., 2012. "Translaminar fracture toughness testing of composites: A review". *Polymer Testing*, Vol. 31, No. 3, pp. 481–489. ISSN 01429418.

Malyszko, L. and Rutkiewicz, A., 2017. "The shear behaviour of pine wood in the Arcan test with the digital image correlation". *MATEC Web of Conferences*, Vol. 117, No. January. ISSN 2261236X.

Monticeli, F.M., Fuga, F.R. and Donadon, M.V., 2023. "Thin-Walled Structures A systematic review on translaminar fracture damage propagation in fiber-reinforced polymer composites". *Thin-Walled Structures*, Vol. 187, No. November 2022, p. 110742. ISSN 0263-8231.

Nikbakht, M. and Choupani, N., 2008. "Fracture Toughness Characterization of Carbon-Epoxy Composite using Arcan Specimen". *Aerospace Engineering*, , No. September, pp. 247–253.

Rikards, R., Buchholz, F.G., Wang, H., Bledzki, A.K., Korjakin, A. and Richard, H.A., 1998. "Investigation of mixed mode I/II interlaminar fracture toughness of laminated composites by using a CTS type specimen". *Engineering Fracture Mechanics*, Vol. 61, No. 3-4, pp. 325–342. ISSN 00137944.

Souza, R.R., Nascimento Junior, S.L., Silveira, N.N., Arbelo, M.A. and Donadon, M.V., 2019. "Translaminar fracture toughness and fatigue crack growth characterization of carbon-epoxy plain weave laminates". *Polymer Composites*, Vol. 40, No. 10, pp. 3791–3804. ISSN 0272-8397.

Ud Din, I., Hao, P., Panier, S., Khan, K.A., Aamir, M., Franz, G. and Akhtar, K., 2020. "Design of a New Arcan Fixture for In-plane Pure Shear and Combined Normal/Shear Stress Characterization of Fiber Reinforced Polymer Composites". *Experimental Techniques*, Vol. 44, No. 2, pp. 231–240. ISSN 17471567.

Williams, M.L., 1961. "On the Stress Distribution at the Base of a Stationary Crack". *Journal of Applied Mechanics*, Vol. 28, No. 1, pp. 78–82. ISSN 0021-8936.

Xu, X., Sun, X. and Wisnom, M.R., 2021. "Initial R-curves for trans-laminar fracture of quasi-isotropic carbon/epoxy laminates from specimens with increasing size". *Composites Science and Technology*, Vol. 216, No. July, p. 109077. ISSN 02663538.

7. RESPONSIBILITY NOTICE

The authors are solely responsible for the printed material included in this paper.